SLAC-PUB-2749
ANL-HEP-PR-81-14
May 1981
(M)

DIRECT COUPLING OF THE PION IN LARGE p_T JET INTERACTIONS*

Edmond L. Berger
High Energy Physics Division
Argonne National Laboratory
Argonne, IL 60439

and

Stanley J. Brodsky
Stanford Linear Accelerator Center
Stanford University
Stanford, California, 94305

ABSTRACT

We emphasize a new class of high transverse momentum hadronic collisions in which the entire energy of an incident meson is delivered into production of a pair of large p_T jets at large angle, with no final state particles emerging along the beam axis. Simple two-body kinematics govern the reaction, with the longitudinal and transverse momentum of the second jet being specified uniquely in terms of those of the trigger jet. The QCD subprocess which mediates the collision involves the direct coupling of the incident meson, and it is normalized absolutely in terms of the pion form factor $F_\pi(Q^2)$.

Submitted to Physical Review D

---

*Work supported in part by the Department of Energy, contracts DE-AC03-76SF00515 and W-31-109-ENG-38.

In recent analyses of high energy data, evidence has emerged in appropriate regions of phase space for an important contribution from high-twist QCD terms in which pions couple directly in the constituent scattering subprocesses. In the Drell-Yan reaction $\pi N \to \gamma^* X$, the high-twist term is observed as a dominant longitudinal polarization[1,2] of the γ^* as the longitudinal momentum $x_F \to 1$. Likewise, in $\nu N \to \mu^- \pi^+ X$, an important $(1-y)$ component [3,4] of $d\sigma/dy$ is identified for large values of $z_\pi = E_\pi/\nu = p_\pi \cdot p_N / Q \cdot p_N$. In this paper, we show that direct QCD coupling of the incident meson in meson-nucleon collisions leads to very special events in which a pair of high p_T jets are produced at large angle with (a) no final state jet along the beam direction, and (b) highly constrained large p_T jet-jet kinematics, such that the longitudinal and transverse momentum of the second jet are specified uniquely by those of the observed (trigger) jet. The general high-twist QCD process we have in mind is sketched in Fig.1(a). It may be contrasted with the conventional leading-twist QCD scattering illustrated in Fig.1(b), in which the two large p_T jets are produced along with spectator jets along the beam and target axis directions.

The two QCD subprocesses which we consider explicitly are

$$\pi q_N \to gq \tag{1}$$

and

$$\pi g_N \to q\bar{q} \ . \tag{2}$$

In reactions (1) and (2), the initial quark, q_N, and gluon, g_N, are constituents of the nucleon target. We ignore $\pi \bar{q}_N \to gq$ because the density of antiquarks $(\bar{q}(x))$ in the nucleon target is insignificant in the region of

relatively large x which contributes to production at large p_T. We consider only contributions from the minimal $|q\bar{q}\rangle$ Fock state of the pion. Contributions from higher Fock states such as $|q\bar{q}g\rangle$ and $|q\bar{q}q\bar{q}\rangle$ provide more complex final states, including beam jets.

As in the case of large momentum transfer exclusive processes,[5] the higher twist amplitude $M(\pi q_N \to gq)$ can be factored into two parts:

(a) the distribution amplitude, $\phi(z,Q)$--the probability amplitude that the valence q and $\bar{q}$ in the pion carry fractions z_1 and z_2 ($z_1 + z_2 = 1$) of the pion's momentum, and are collinear up to transverse momenta $k_{\perp i} \sim Q$, where Q is the typical momentum transfer in the subprocess; and

(b) the hard-scattering amplitude T_H for scattering the quarks and gluons in the subprocess $q\bar{q} + q_N \to g + q$, where the q and $\bar{q}$ are collinear with the initial pion.

We thus obtain the invariant amplitude for $\pi q_N \to gq$:

$$M(\hat{s},\hat{t}) = \int_0^1 dz_1 \int_0^1 dz_2 \, \phi_\pi(z_i,Q)\delta(1-z_1-z_2)T_H(\hat{s},\hat{t};z_i) \, . \qquad (3)$$

All of the effects of hadronic binding are contained in the distribution amplitude ϕ. If we neglect power law corrections in $1/Q$, the external lines in T_H can be taken as massless. Sketched in Fig.2 are the five QCD Feynman Born diagrams which contribute to reactions (1) and (2), to leading order in $\alpha_s(Q^2)$. They are identical to the gauge-invariant set studied in detail in Ref.6. The QCD radiative corrections associated with the q_N and g_N lines lead to the standard Q^2 evolution for the quark and gluon structure functions.

Specific labeling of momenta for the T_H Born diagrams is shown in

Fig.2(a). The quark and antiquark constituents of the pion are constrained to form a pseudoscalar, color singlet state. The pseudoscalar projection is achieved in the invariant amplitude via the substitution

$$\frac{1}{\sqrt{2}}\left[u_-(z_1p_\pi)\bar{v}_+(z_2p_\pi) - u_+(z_1p_\pi)\bar{v}_-(z_2p_\pi)\right] = \frac{1}{\sqrt{2}}\not{p}_\pi\gamma_5 \ . \tag{4}$$

All five diagrams in Fig.2 carry the same color factor $-T^a_{ij}/6\sqrt{3}$, where $\underline{i}$ and $\underline{j}$ label the color indices of the final and initial quarks, in Fig.2, and $\underline{a}$ labels the final gluon. We define the subprocess invariants $\hat{s} = (p_1 + p_5)^2 = (p_2 + p_\pi)^2$; $\hat{t} = (p_1 - p_2)^2$; and $\hat{u} = (p_1 - p_\pi)^2$.

After deriving explicit Feyman amplitudes for the gauge-invariant set of graphs in Fig.2, and simplifying the result, we obtain[6]

$$T_H(\pi q_N \to gq) = \frac{ig^3T^a_{ij}}{6\sqrt{6}}\frac{1}{z_1z_2\hat{s}\hat{t}\hat{u}}\tilde{M}^\mu\varepsilon_\mu \ , \tag{5}$$

where

$$\tilde{M}^\mu = A\,\bar{u}(p_1)\gamma_5\gamma^\mu u(p_2) + B^\mu\bar{u}(p_1)\gamma_5\not{p}_\pi u(p_2) \ . \tag{6}$$

The functions A and B are expressed as

$$A = 8\hat{t}(\hat{s} - \hat{u}) \ ; \tag{7}$$

$$B^\mu = 32\hat{u}p_1^\mu + 32\hat{s}p_2^\mu - 18(\hat{s} - \hat{u})p_5^\mu + 16(\hat{s} - \hat{u})p_\pi^\mu \ . \tag{8}$$

One may check that $p_5 \cdot B = -A$, and, therefore,

$$p_5^\mu\tilde{M}^\mu = 0 \ , \tag{9}$$

as is required by gauge invariance. The isospin symmetry of the distribution amplitude $\phi(z_i)$ in Eq.(3) permits us to retain in Eqs.(7) and (8) only those terms symmetric in z_1 and z_2. Thus, our Eqs.(7) and (8) differ slightly from those presented in Ref.6, where the symmetry was ignored.

The form of Eq.(3) may be compared with that appropriate for the form factor of the pion[5] at large Q^2:

$$F_\pi(Q^2) = \int\int dx_i \delta(1 - x_1 - x_2) \int\int dy_i \delta(1 - y_1 - y_2) \phi^*(x_i,Q)\phi(y_i,Q) \times \frac{16\pi\alpha_s(Q^2)}{3Q^2 x_1 x_2 y_1 y_2} . \tag{10}$$

Here, as usual, $\alpha_s = g^2/4\pi$. We note that the distribution amplitude $\phi(z_i,Q)$ enters Eq.(3 and 5) and Eq.(10) with the same weight factor $(1/z_1 z_2)$. This implies that the cross-sections for $\pi q_N \to qg$ and $\pi g_N \to q\bar{q}$ may be normalized absolutely in terms of data on $F_\pi(Q^2)$, <u>entirely independently of assumptions about the specific functional form of $\phi(z_i,Q)$</u>.

From Eqs.(5-8), we obtain the spin- and color-averaged squared matrix element

$$\frac{1}{6} \sum_{\text{colors,spin}} |M(\hat{s}, \hat{t}, \hat{u})|^2 = g^6 \frac{64}{81} \left[-\frac{\hat{t}}{\hat{s}^2} - \frac{\hat{t}}{\hat{u}^2}\right] \left| \int_0^1 \frac{\phi_\pi(z,Q)dz}{z(1-z)} \right|^2 . \tag{11}$$

Substituting from Eq.(10), we derive

$$\frac{1}{\pi} \frac{d\sigma}{d\hat{t}} (\pi q_N \to gq) = \frac{16}{27} \frac{\alpha_s^2}{\hat{s}^2} F_\pi(\hat{s}) \left[-\frac{\hat{t}}{\hat{s}} - \frac{\hat{t}\hat{s}}{\hat{u}^2}\right] . \tag{12}$$

Equation (12) is correct to leading order in $\alpha_s(\hat{s})$. By relating $\frac{d\sigma}{d\hat{t}}(\pi q_N \to gq)$ to the observed $F_\pi(\hat{s})$, we include correctly in Eq.(12) all of the anomalous dimension $\left(\log Q^2/\Lambda^2\right)^{-\gamma_n}$ contributions from the evolution of the meson distribution amplitude $\phi(z,Q)$. Because Eq.(12) is linear in $\hat{t}$, the cross-section vanishes in the limit that the final gluon emerges along the direction of the incident pion. This result is a simple manifestation of helicity conservation at the $q\bar{q}g$ vertices in Fig.2.

The value of $F_\pi(Q^2)$ is measured[7] for $Q^2 \gtrsim 4$ GeV^2. For the larger values of Q^2, it may be parametrized as $F_\pi(Q^2) = 0.4$ GeV$^2/Q^2$, $Q^2 > 2$ GeV^2, and we use this analytic expression to obtain numerical predictions in this paper. Alternatively, one could adopt an explicit asymptotic expression[5] $(Q \to \infty)$ for $\phi(z)$ in Eqs.(3) and (10), such as $\phi(z) = \sqrt{3}\, f_\pi z_1 z_2$, where f_π is the pion weak decay constant, $f_\pi = 93$ MeV. With this form, $F_\pi(Q^2) = 16\pi\, \alpha_s(Q^2) f_\pi^2/Q^2$, and Eq.(12) is replaced by

$$\frac{1}{\pi}\frac{d\sigma}{d\hat{t}}(\pi q_N \to gq) \to 4\pi\, \alpha_s^3 \frac{64}{27}\frac{f_\pi^2}{\hat{s}^3}\left[\frac{-\hat{t}}{\hat{s}} - \frac{\hat{t}\hat{s}}{\hat{u}^2}\right] . \qquad (13)$$

Using the asymptotic expression for $\phi(z)$ and $\alpha_s = 0.3$, one underestimates $F_\pi(Q^2)$ by roughly a factor of three at $Q^2 \simeq 4$ Gev^2. Correspondingly, use of Eq.(13), with $f_\pi = 93$ MeV, instead of Eq.(12) yields predictions for inclusive jet cross-sections which are a factor of three lower than those we present.

For $\pi g_N \to q\bar{q}$ we derive

$$\frac{1}{\pi}\frac{d\sigma}{d\hat{t}}(\pi g_N \to q\bar{q}) = \frac{2}{9}\frac{\alpha_s^2}{\hat{s}^2}F_\pi(\hat{s})\left[\frac{\hat{s}^2}{\hat{u}^2}+\frac{\hat{s}^2}{\hat{t}^2}\right] + 4\pi\,\alpha_s^3\,\frac{8}{9}\frac{f_\pi^2}{\hat{s}^3}\left[\frac{\hat{s}^2}{\hat{u}^2}+\frac{\hat{s}^2}{\hat{t}^2}\right] \tag{14}$$

where now $\hat{s} = (p_q + p_{\bar{q}})^2$.

The factor $\hat{s}^{-3}$ in Eqs.(13) and (14) implies that (1) and (2) provide contributions to the jet yield $Ed\sigma/d^3p$ which have the high-twist form $p_T^{-6}f(x_F,x_T)$, rather than the leading-twist p_T^{-4} behavior. Here, as usual, $x_T = 2p_T/\sqrt{s}$ and $x_F = 2p_L^{c.m.}/\sqrt{s}$. The cross-sections in Eqs.(12) and (14) are smaller than typical $2 \to 2$ QCD constituent scattering cross-sections by a factor of order $F_\pi(p_T^2)$.

To obtain estimates of the expected size of our high-twist jet production yields, we multiply Eqs.(12) and (14) by appropriate quark and gluon distribution functions. For $\pi^- p \to gqX$, we obtain

$$\frac{Ed\sigma}{d^3p} = x\,u_N(x)\left(\frac{s}{s+u}\right)\frac{1}{\pi}\frac{d\sigma}{d\hat{t}}(\pi q_N \to gq)\ , \tag{15}$$

where $u_N(x)$ is the probability that an up quark in the proton carries momentum fraction $x = \hat{s}/s$. There is no integral to perform in Eqs.(15); at fixed $s = (p_\pi + p_N)^2$, $\hat{s}$, $\hat{t}$, and x are specified uniquely by the jet momentum p; $u = (p-p_N)^2$. As long as the appropriate kinematic identification is made in relating $\hat{t}$ and p, Eq.(15) applies to production of either a final gluon jet or a final (down) quark jet.

For $\pi p \to q\bar{q}X$, the inclusive q or $\bar{q}$ jet yield is provided by

$$\frac{Ed\sigma}{d^3p} = xG(x)\left(\frac{s}{s+u}\right)\frac{1}{\pi}\frac{d\sigma}{d\hat{t}}(\pi g_N \to q\bar{q}X)\ , \tag{16}$$

where $G(x)$ is the gluon density in the proton. We select simple distribution functions suggested by constituent counting rules[8], $xG(x) = 3(1-x)^5$ and $xu_N(x) = (1-x)^3$, normalized such that the gluons and up quarks carry respectively 50% and 25%, of the proton momentum. More detailed parametrizations including Q^2 evolution will not affect our qualitative conclusions, but they may be warranted when future comparisons are made with relevant data. We adopt the constant value $\alpha_s = 0.3$.

In Fig.3 we present our predicted inclusive jet yield as a function of the jet transverse momentum p_T for $\pi^- p \to$ jet X at $\sqrt{s} = 20$ GeV and πp center-of-mass jet angle $\theta^* = 45°$. The maximum value of p_T is $p_T^{max} = \frac{\sqrt{s}}{2} \sin\theta^* \approx 7$ GeV. Also shown in Fig.3 is the decomposition of the cross-section into contributions from the different QCD subprocesses. At 45°, the contribution from the initial gluon process is dominant as long as $p_T \lesssim 5.5$ GeV. The probability is greatest that the detected jet is a (down) quark jet, rather than an antiquark or gluon jet. This probability also increases with p_T.

In Fig.4 we present a prediction of the center-of-mass angular dependence of the inclusive yield at a fixed value of p_T, chosen to be $p_T = 4.5$ GeV. As θ^* is reduced, the yield falls to zero as the kinematic limit $\sin\theta^* = 2p_T/\sqrt{s}$ is approached. The rate of decrease reflects both the x dependence of the nucleon constituent distribution functions as well as dynamical factors in the constituent scattering cross-sections, Eqs.(12) and (14). The helicity conservation factor $\hat{t}$ in Eq.(12) suppresses gluon jet production at small θ^*, and $\pi^- u \to dg$ is favored over $\pi^- g \to d\bar{u}$ at small angles because the initial quark density is harder than the initial gluon densities.

In Fig.5, we present the scaling distribution $p_T^6 \, Ed\sigma/d^3p$ as a function of x_T for both $\theta^* = 45°$ and $90°$. From this figure predictions may be obtained for $\pi^- p \to$ jet X at any desired energy.

For $\pi^{\pm} p \to$ jet X, the initial gluon contributions are identical, but $\sigma(\pi^+ d_N \to ug) \simeq \frac{1}{2} \sigma(\pi^- u_N \to dg)$. We also expect

$$\frac{Ed\sigma}{d^3p}(K^- p \to \text{jet}X) \simeq \left(\frac{f_K}{f_\pi}\right)^2 \frac{Ed\sigma}{d^3p}(\pi^- p \to \text{jet X}) \tag{17}$$

where $(f_K/f_\pi)^2 \simeq 1.45$, but $K^+ p \to$ jetX receives contributions only from the initial gluon subprocess $K^+ g \to u\bar{s}$. The angular dependence shown in Fig.4 and various sums and differences of cross-sections may be exploited to accentuate contributions from different subprocesses. If a clean high-twist signal is isolated, the overall energy dependence of the inclusive yield may supply constraints on the x dependence of the initial constituent distribution functions.

When compared with reported inclusive jet yields,[9] the predictions in Figs.3 and 4 account for three to five percent of the experimental signal. Nevertheless, because of the absence of a stream of spectator particles along the beam direction, and because of the unique two body kinematics of processes (1) and (2), it should be possible to isolate the relevant high-twist signals. Conservation of energy and of longitudinal momentum require

$$(E^\pi + p_L^\pi) = (E + p_L)^{\text{jet 1}} + (E + p_L)^{\text{jet 2}} \tag{18}$$

for the high-twist processes we are considering ($s \gg m_N^2$). Once p_T and p_L are determined for the first (trigger) jet, those of the recoil jet are

fixed. Since the entire four momentum of the incident pion is delivered to the QCD subprocess, there is no smearing of the jet kinematics associated with a spread of the incident hadron constituent longitudinal momentum. Smearing associated with intrinsic transverse momentum of the initial constituents is also reduced since only one initial constituent is present. In terms of light-cone momentum fractions defined as

$$\omega_{\text{jet } i} = \left(E^i + p_L^i\right) \Big/ \left(E^\pi + p_L^\pi\right) , \tag{19}$$

the events of interest are those for which $\omega_1 + \omega_2 \simeq 1$. Since ω_{jet} is the sum of the individual ω_k for each hadron component in the jet, the events of interest may also be defined as those for which $\sum \omega_k = 1$, summed over both jets.

We advocate a detailed analysis of high p_T jet events in which a veto is imposed to exlcude "normal" events, illustrated in Fig.1(b), in which hadron energy emerges along the beam axis. For this sample, we provide an absolutely normalized prediction for the yield of events in which $\omega_1 + \omega_2 = 1$. Kinematically, these events are analogous to the leading-twist high-p_T events in $\gamma p \to$ jet X, associated with the pointlike coupling of the photon. In $\pi N \to$ jet X, however, the events are generated by a pointlike, short-distance coupling of the pion in the Q.C.D. subprocess. Observations of this class of events in $\pi N \to$ jet X will provide a significant verification of the applicability of the Fock state decomposition of the pion wave function into color singlet $|q\bar{q}\rangle$ and higher components. The high p_T jet events without hadron energy along the beam axis direction measure the amplitude associated with this $|q\bar{q}\rangle$ component. They comprise an event topology which

probes the joint probability for finding both a q and a $\bar{q}$ in the beam, and only a q and $\bar{q}$, a concept ignored in the conventional parton model in which constituents are presumed to act singly and incoherently. Events with no hadron energy radiated along the beam axis direction are possible only because the initial state which participates in the hard scattering (here a pion) is a color singlet.

Regardless of the details of the specific QCD calculation discussed in this paper,[10] it is of important physical interest to ascertain the size of the cross-section associated with the simple event topology which we emphasize. Our focus is on meson induced reactions. Nevertheless, although having no quantitative predictions for processes initiated by nucleon beams, we remark that events without hadron energy along the beam axis may indicate an unlikely subprocess in which the quark-diquark substructure of the nucleon plays the dominant role.

REFERENCES

1. E. L. Berger and S. J. Brodsky, Phys. Rev. Lett. 42, 940 (1979). See also Z. F. Ezawa, Nuovo Cimento 23A, 271 (1974) and G.R. Farrar and D. R. Jackson, Phys. Rev. Lett. 35, 1416 (1975).
2. K. J. Anderson et al., Phys. Rev. Lett. 43, 1219 (1979).
3. E. L. Berger, Phys. Lett. 89B, 241 (1980) and Z. Phys. C4, 289 (1980).
4. M. Haguenauer et al., Phys. Lett. 100B, 185 (1981).
5. G. P. Lepage and S. J. Brodsky, Phys. Rev. D22, 2157 (1980) and references therein. See also A. V. Efremov and A. V. Radyushkin, Phys. Lett. 94B, 245 (1980); and A. Duncan and A. Mueller, Phys. Rev. D21, 1636 (1980).
6. E. L. Berger, T. Gottschalk, and D. Sivers, Phys. Rev. D23, 99 (1981). For related higher-twist photon processes, see S. J. Brodsky, J. F. Gunion, and R. Rückl, Phys. Rev. D18, 2469 (1978), and J. Bagger and J. F. Gunion, to be published.
7. C. J. Bebek et al., Phys. Rev. D13, 25 (1976).
8. S. J. Brodsky and G. R. Farrar, Phys. Rev. Lett. 31, 1153 (1973). R. Blankenbecler and S. J. Brodsky, Phys. Rev. D10, 2973 (1974).
9. C. Bromberg et al., Phys. Rev. Lett. 43, 565 (1979) and references therein; M. Dris et al., Phys. Rev. D19, 1361 (1979) and references therein.
10. Contributions from the QCD subprocess $\pi q \to \pi q$ were studied earlier by G. Farrar and G. C. Fox, Nucl. Phys. B167, 205 (1980). These authors employ a normalization procedure consistent with ours.

FIGURE CAPTIONS

1. (a) Illustration of $\pi N \to gdX$ via the QCD subprocess $\pi u \to gd$. The unshaded oval represents the full QCD hard-scattering amplitude for $\pi u \to gd$.

   (b) Illustration of $\pi N \to cdX$ via the QCD subprocess $\underline{a}\,\underline{b} \to \underline{c}\,\underline{d}$, where $\underline{a}$ and $\underline{b}$ are constituents of the π and N respectively.

2. Full set of QCD Feynman graphs for $\pi + q(p_2) \to g(p_5) + q(p_1)$.

3. Jet transverse momentum dependence of the predicted inclusive jet yield $Ed\sigma/d^3p$ for $\pi^- p \to jetX$ at $\sqrt{s} = 20$ GeV and center-of-mass jet angle $\theta^* = 45°$, measured with respect to the incident pion direction. Shown is the total jet yield and the component contributions from the QCD subprocesses $\pi^- g_N \to \bar{u}d$ and $\pi^- u_N \to dg$. For the component reactions, the subscript "t" denotes the observed "trigger" jet which emerges at θ^*.

4. Dependence of the predicted jet yield on the center-of-mass scattering angle θ^* at $\sqrt{s} = 20$ GeV and $p_T = 4.5$ GeV.

5. Dependence of the product $p_T^6\, Ed\sigma/d^3p$ on the scaling variable $x_T = 2p_T/\sqrt{s}$ for $\theta^* = 45°$ and $90°$. These results are valid for any chosen value of $\sqrt{s}$.

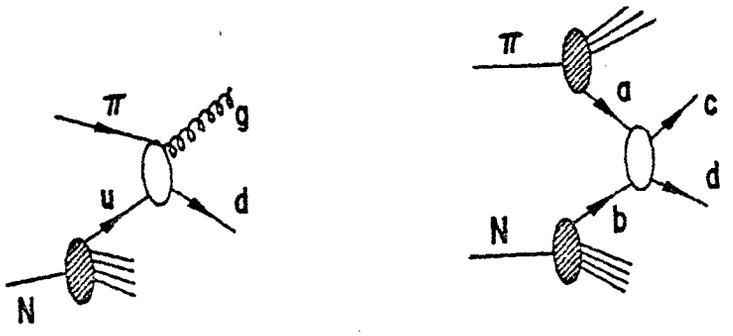

Fig. 1

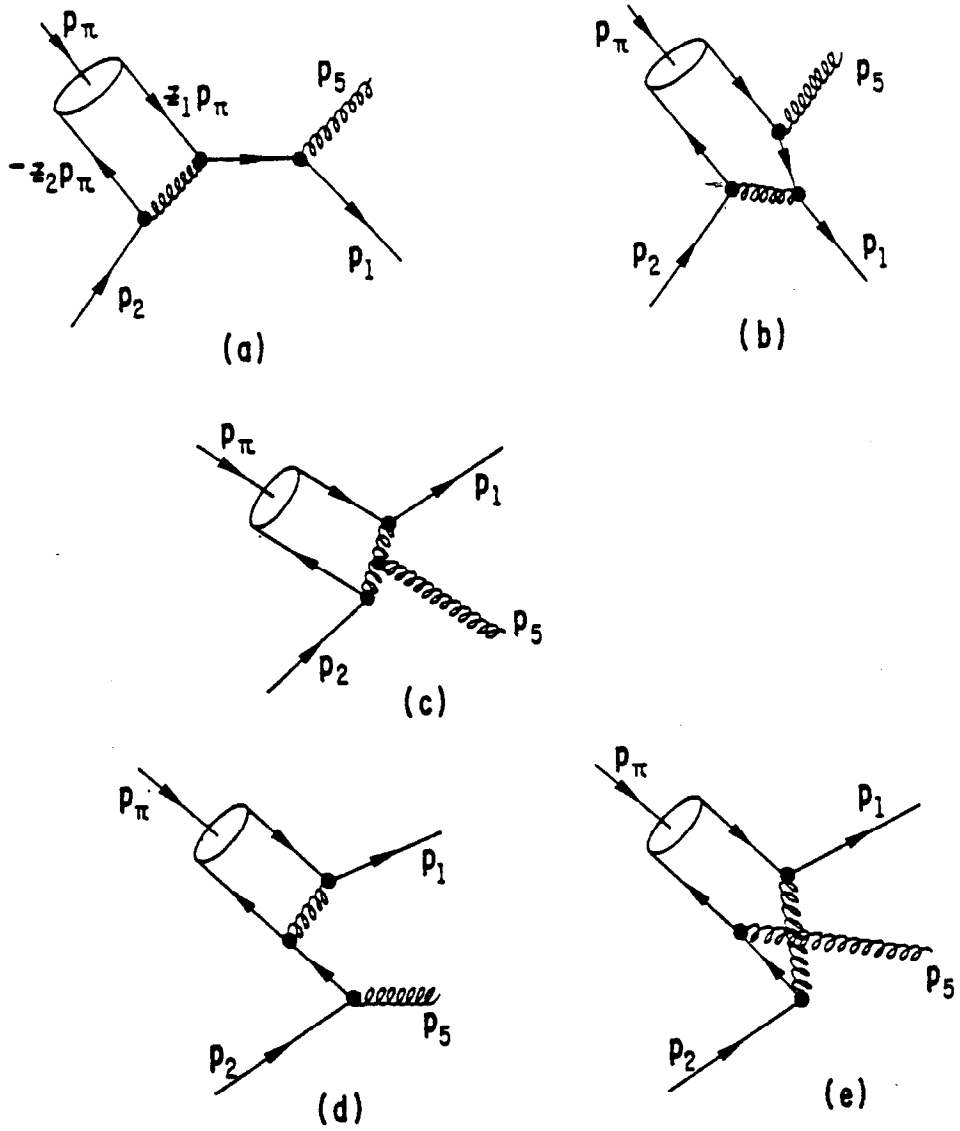
p_π
$z_1 p_\pi$
$-z_2 p_\pi$
p_5
p_1
p_2
(a)
p_π
p_5
p_2
p_1
(b)
p_π
p_1
p_5
p_2
(c)
p_π
p_1
p_5
p_2
(d)
p_π
p_1
p_5
p_2
(e)

Fig. 2

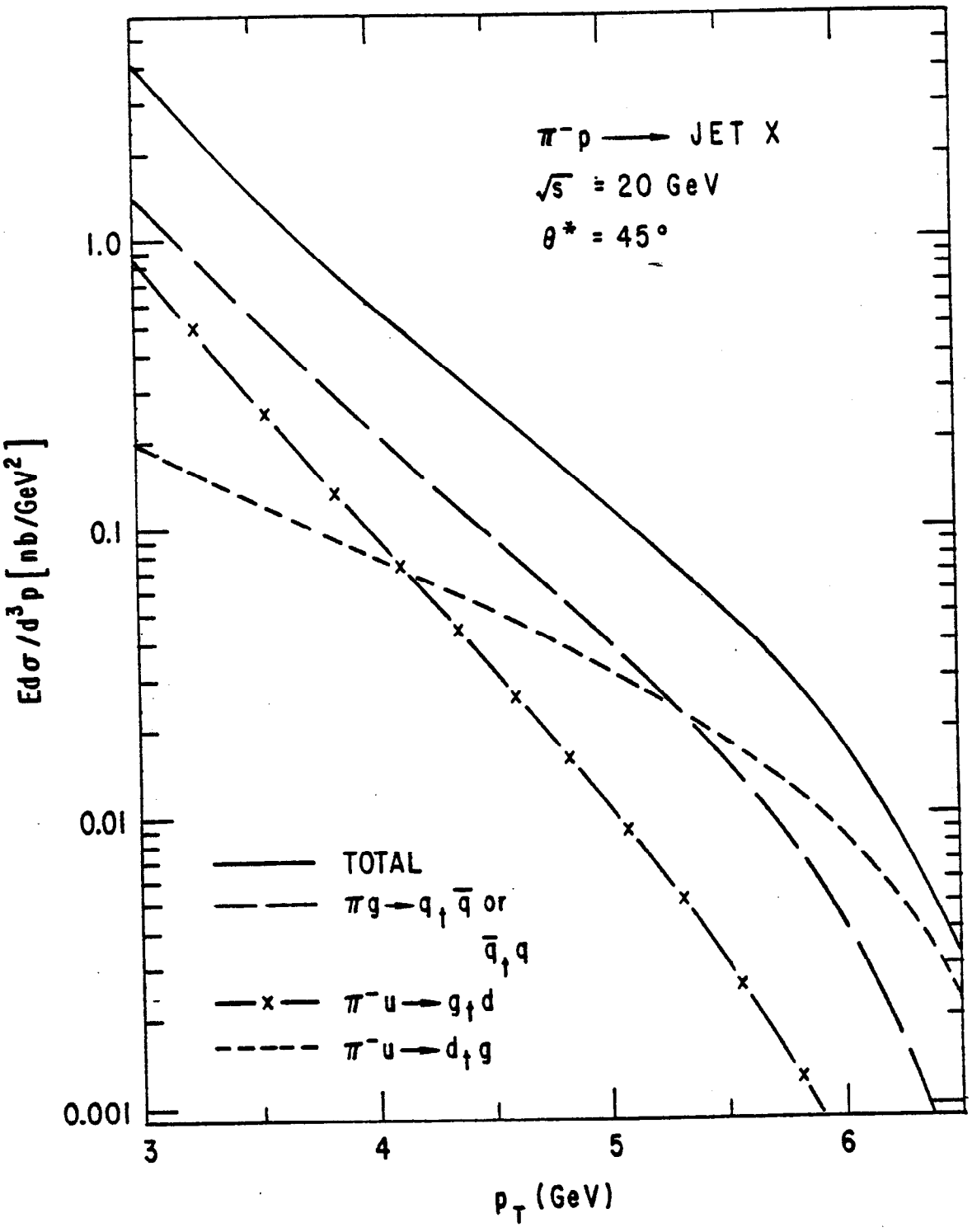
$\pi^- p \longrightarrow$ JET X
$\sqrt{s}$ = 20 GeV
θ^* = 45°
TOTAL
$\pi g \to q_f \bar{q}$ or $\bar{q}_f q$
$\pi^- u \to g_f d$
$\pi^- u \to d_f g$
$E d\sigma/d^3p$ [nb/GeV^2]
1.0
0.1
0.01
0.001
3
4
5
6
p_T (GeV)

Fig. 3

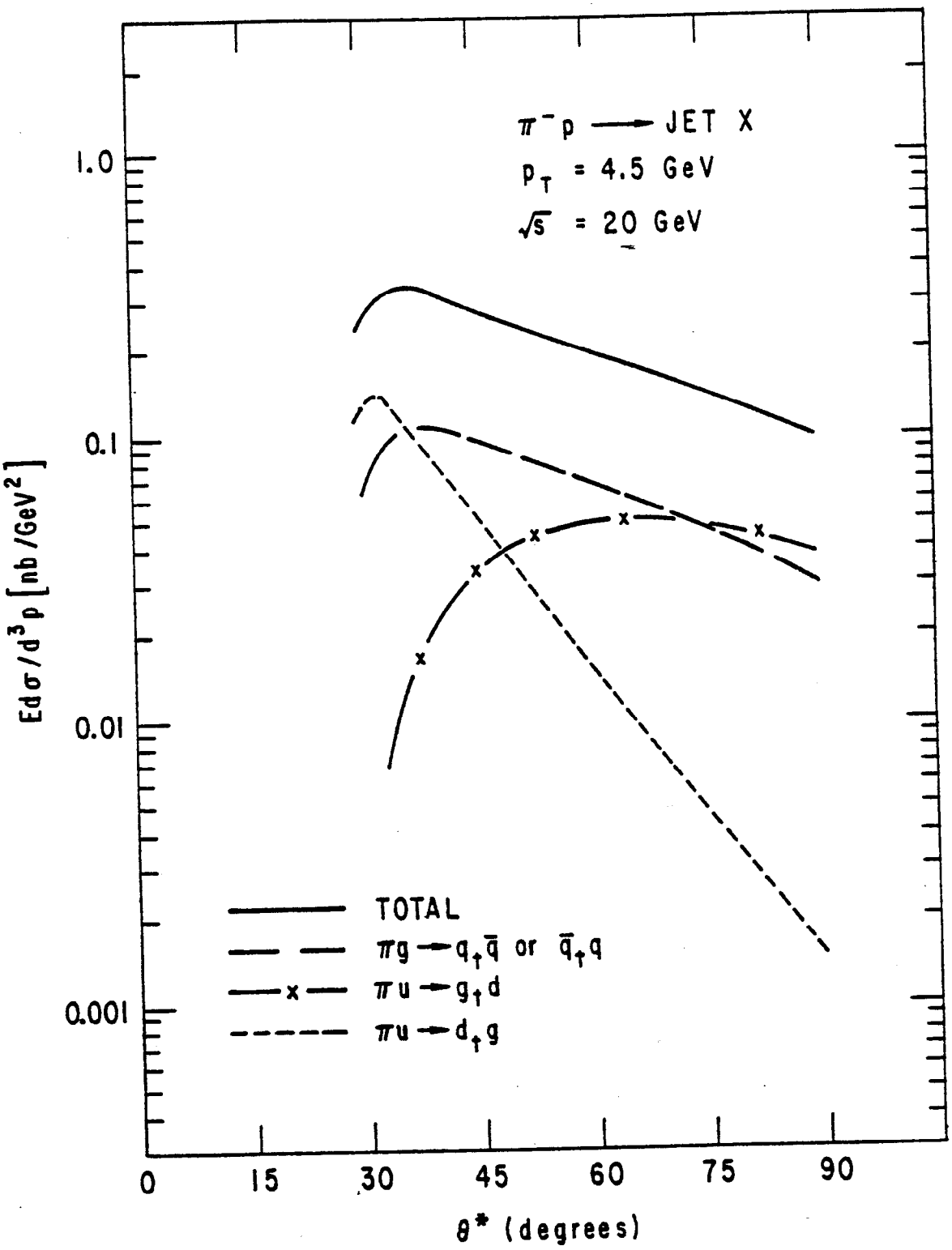
$\pi^- p \longrightarrow$ JET X
p_T = 4.5 GeV
$\sqrt{s}$ = 20 GeV
TOTAL
$\pi g \rightarrow q_f \bar{q}$ or $\bar{q}_f q$
$\pi u \rightarrow g_f d$
$\pi u \rightarrow d_f g$
$E d\sigma/d^3p$ [nb/GeV^2]
1.0
0.1
0.01
0.001
0
15
30
45
60
75
90
θ^* (degrees)

Fig. 4

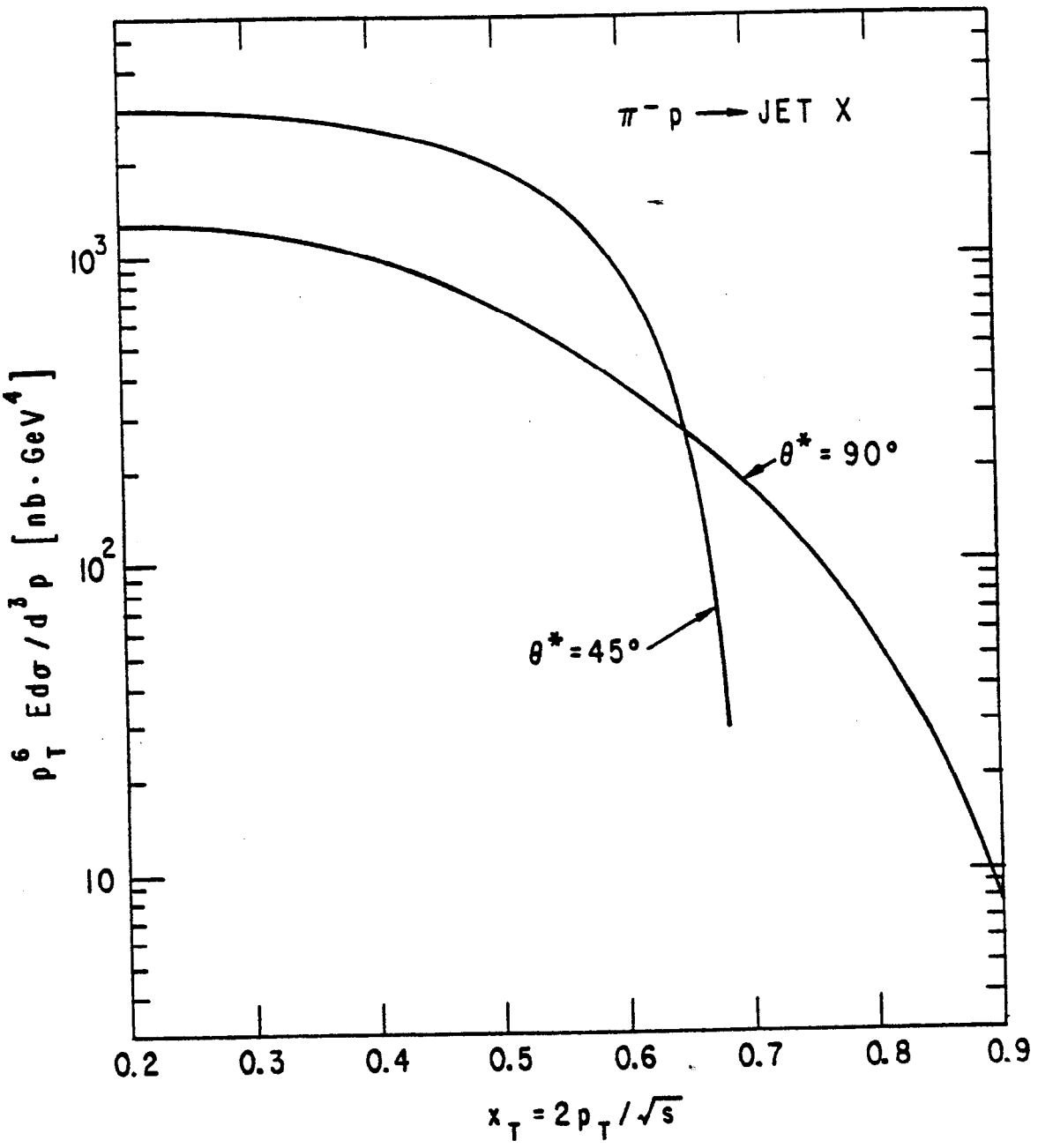
$\pi^- p \longrightarrow$ JET X
$\theta^* = 90°$
$\theta^* = 45°$
$p_T^6 \, E d\sigma / d^3p$ [nb · GeV^4]
10^3
10^2
10
0.2
0.3
0.4
0.5
0.6
0.7
0.8
0.9
$x_T = 2p_T / \sqrt{s}$

Fig. 5